Accepted by the Astronomical Journal
Preprint typeset using LaTeX style emulateapj v. 25/04/01

ASSESSING THE FORMATION SCENARIOS FOR THE DOUBLE NUCLEUS OF M31 USING TWO-DIMENSIONAL IMAGE DECOMPOSITION[1]

Chien Y. Peng[2]
Accepted by the Astronomical Journal

ABSTRACT

The double nucleus geometry of M31 is currently best explained by the eccentric disk hypothesis of Tremaine, but whether the eccentric disk resulted from the tidal disruption of an inbounding star cluster by a nuclear black hole, or by an $m = 1$ perturbation of a native nuclear disk, remains debatable. I perform detailed 2-D decomposition of the M31 double nucleus in the *Hubble Space Telescope* V-band to study the bulge structure and to address competing formation scenarios of the eccentric disk. I deblend the double nucleus (P1 and P2) and the bulge simultaneously using five Sérsic and one Nuker components. P1 and P2 appear to be embedded inside an intermediate component ($r_e = 3\farcs2$) that is nearly spherical ($q = 0.97 \pm 0.02$), while the main galaxy bulge is more elliptical ($q = 0.81 \pm 0.01$). The spherical bulge mass ($2.8 \times 10^7 M_\odot$), being coincident with the supermassive black hole mass ($3 \times 10^7 M_\odot$), conjoined with a shallow bulge cusp, are consistent with the scenario that the bulge was scoured by spiraling binary supermassive black holes. In the 2-D decomposition, the bulge is consistent with being centered near the UV peak of P2, but the exact position is difficult to pinpoint because of dust in the bulge. P1 and P2 are comparable in mass. Within a radius $r = 1''$ of P2, the relative mass fraction of the nuclear components is $M_\bullet : M_{bulge} : P1 : P2 = 4.3 : 1.2 : 1 : 0.7$, assuming the luminous components have a common mass-to-light ratio of 5.7. The eccentric disk as a whole (P1+P2) is massive, $M \approx 2.1 \times 10^7 M_\odot$, comparable to the black hole and the local bulge mass. As such, the eccentric disk could not have been formed entirely out of stars that were stripped from an inbounding star cluster. Hence, the more favored scenario is that of a disk formed in situ by an $m = 1$ perturbation, caused possibly by the passing of a giant molecular cloud, or the passing/accretion of a small globular cluster.

Subject headings: fundamental parameters – technique: photometry – galaxies: structure, nucleus – individual: M31

1. INTRODUCTION

M31 is the nearest galaxy with a normal bulge where there is good evidence for the existence of a supermassive black hole (SBH) of $M_\bullet \approx 3 \times 10^7 M_\odot$ (e.g. Kormendy & Bender 1999; Kormendy 1987; Dressler & Richstone 1988; Richstone, Bower, & Dressler 1990). Early Stratosphere II balloon observations (Light et al. 1974) saw that M31 appeared to have a dense nucleus embedded on top a galaxy bulge. Nieto et al. (1986) showed that the nucleus was off centered slightly from the bulge and asymmetric, which was hinted at in Light et al. (1974). It was not until *HST (Hubble Space Telescope)* WFPC (Wide Field and Planetary Camera) and FOC (Faint Object Camera) observations, that the nucleus was resolved into double components (Lauer et al. 1993 [L93]; King, Stanford, & Crane 1995 [K95]; Lauer et al. 1998 [L98]).

Figure 1 shows a grey scale V-band ($F555W$) image of the nucleus from *HST* WFPC2 in V, which was deconvolved and kindly provided by T. Lauer (see L98). The brighter of the double peak in the V-filter is designated as P1, and it is separated from the fainter P2 by $0\farcs49$, or 1.8 pc (L93). In the far-UV, however, K95 discover that P2 is actually more luminous than P1. There is a striking UV peak (upturn) on top of P2 which stands apart in color from both P2 and P1. In literature, P2 is synonymous with the UV peak, but here I make the distinction because the peak is not centered on P2, as shown later. In the infrared, the contrast between the two nucleus is not quite as strong as in the optical, and the peak seen in UV-light all but disappears, either because it is intrinsically faint or is smeared away by the PSF (Corbin, O'Neil, & Rieke 2001). Dust is ruled out as being the cause for the appearance and asymmetry of the double nucleus based on color images of the optical, far-UV, and near-infrared H-K (Corbin, O'Neil, & Rieke 2001; Mould et al. 1989), as well as a two-dimensional decomposition by K95, who impose the assumption that both P1 and P2 components are smooth.

Despite the prominence of P1 in optical images, L93 and L98 show that it is the UV peak which corresponds more closely to the center of the galaxy bulge, using isophotal centroids. They also suggest it is the location of the SBH. From rotation curves, Kormendy & Bender (1999 [KB99]), Bacon et al. (2001 [BA01]), and Statler et al. (1999 [S99]) find that the UV peak of P2 also lies close to the dynamical center. The most precise measurements put the zero-velocity center at $0\farcs051 \pm 0\farcs014$ (KB99) and $0\farcs031$ (BA01) from the UV peak of P2, in the direction of P1. However, the peak of the velocity dispersion is $0\farcs2$ from P2, *away* from P1 (KB99, BA01). KB99 locate the SBH near the center of the UV peak.

K95 speculate that the strong UV peak may be due to a non-thermal, low-level, active galactic nucleus (AGN), coincident with X-ray and radio emissions, but acknowledge it is unclear whether it is truly resolved in pre-COSTAR

[1] Based on observations with the NASA/ESA *Hubble Space Telescope*, obtained at the Space Telescope Science Institute, which is operated by AURA, Inc., under NASA contract NAS 5-26555.

[2] Steward Observatory, University of Arizona, 933 N. Cherry Ave., Tucson, AZ 85721. cyp@as.arizona.edu

HST images. Moreover, it has the energy output of only a single post asymptotic giant star (K95). L98 find that the UV peak is resolved by *HST* WFPC2, leading them to hypothesize that the bluish color may not be an AGN, but instead is caused by a population of late B to early A-type stars in a cluster, possibly in a region with high metallicity abundance (e.g. Burstein et al. 1988, and K95). Forming such a cluster may be difficult, however, because of the tidal influence of a nearby $3 \times 10^7 M_\odot$ black hole. The AGN speculation about the UV peak has not been clarified despite Chandra observations. Garcia et al. (2000) discover X-ray emission in proximity to P2 with an unusual spectrum indicating possible relation to an active nucleus. The error circle, however, is $1''$(twice the separation between P1 and P2), and is not alone – there are a number of other X-ray sources farther away around the bulge. If the UV peak is in fact AGN related, it is curious that it does not have a counterpart in the near-IR where the emissions are often seen more clearly than in the optical due to a typical rise in the AGN spectrum and diminished extinction (Quillen et al. 2001).

Several empirical evidences indicate that the nucleus and the bulge have a different formation history. Within $0\farcs4 \times 0\farcs4$ of P1, L98 show that the color is redder in $V-I$ ($=1.41$) than the surrounding bulge ($V-I=1.34$). But in $U-V$, P1 (=2.29) and its anti-P2 direction ($U-V$=2.18) appear to be bluer than the bulge ($U-V$=2.39). This is in contrast to BA01 who find both P1 and anti-P2 to also be redder. Nonetheless, both their findings indicate that the nucleus has a stellar population, metallicity, and perhaps origins, different from that of stars in the bulge. Sil'chenko, Burenkov, & Vlasyuk (1998 [SBV98]) show that the nucleus is more metal rich than the surrounding. In the two regions, the spectral indices differ by, $\Delta \mathrm{Mg_b} = 0.86 \pm 0.1$ and $\Delta \langle \mathrm{Fe} \rangle = 0.53 \pm 0.08$. KB99 confirm that P1 and P2 have a similar stellar population, have higher metal line strengths, and are more similar to each other than to the bulge or to any globular cluster. SBV98 also use $[\mathrm{H}\beta / \langle \mathrm{Fe} \rangle]$ to show that stars in the nucleus are younger by roughly $\lesssim 8$ Gyrs.

The compactness of the P1 and P2 peaks is particularly interesting and challenging to explain from the standpoint of galaxy formation and dynamical evolution. KB99 determine the combined mass of the double nucleus to be $M_{nuc} \simeq 3.5 \times 10^7 M_\odot$, comparable to the mass of the SBH. That such a configuration exists at all with such close separation (1.7 pc) is surprising, and a natural interpretation is that P1 is either a merger remnant or a captured star cluster. Emsellem & Combes (1997) model this scenario with N-body simulations in a SBH potential and find that, although they can reproduce the geometry, the lifetime is on the order of 0.5 Myr. If the cluster is massive enough to survive disruption, in most cases, dynamical friction would cause P1 to spiral in and coalesce with P2 within several dynamical times, unless somehow P1 co-rotates with the bulge (K95). Although the short life span of an accreting scenario is not in itself conclusive proof, the discovery of other similar such systems (e.g. NGC 4486B, Lauer et al. 1996) favors a scenario which has a much longer lifespan. Moreover, S99 find that the sinking star cluster of Emsellem & Combes (1997) model does not reproduce either the rotation curve or the dispersion profile.

Tremaine (1995) proposes an eccentric disk model to explain the nuclear configuration which currently stands as the favorite model. The thick eccentric disk, nearly Keplerian, is composed of stars in ring orbits around a black hole, and P1 is caused by a bottleneck of stars slowing down at the turnaround radius (apocenter). This model also predicts that the velocity center is displaced by $\sim 0\farcs2$ from P2 in the direction of P1. Moreover, it predicts that the stars in P1 and P2 should have a similar stellar population because they belong to the same system, which might not be the case if P1 is a merger remnant. With spectroscopic data, KB99 show that the shift of the rotation center is in the right sense of the prediction, even if the amount is somewhat lower than prediction. Moreover, P1 and P2 have more similar stellar populations to each other than to the bulge in accord with the model prediction. However, the missing element in the Tremaine model is an explanation for how the ring orbits maintain alignment under precession: the original model has no self gravity. Since then, several workers have proposed enhancements. Among them, Salow & Statler (2001) propose a semi-analytic eccentric disk with self-gravity around a black hole, where the disk is made up of a superposing set of Keplerian orbits dispersed in eccentricity and orientation according to a certain distribution function. It predicts that the line-of-sight velocity distributions of the disk near the black hole should have a distinctive double peak, which provides a further observational constraint to test the eccentric disk model. Using a different formalism, with integrable models, Jalai & Rafiee (2001) show that the double nucleus geometry can be sustained with four general types of regular orbits in a Stäckel potential, even in the absence of a SBH. However, the requirement that the nuclei be cuspy, with surface density $\Sigma \propto r^{-2}$ is a stringent requirement, and is not seen in M31. Furthermore, it is not clear why the nucleus would be asymmetric.

Bekki (2000 [BE00]), BA01, and Sambhus & Sridhar (2001 [SS01]), propose scenarios for how such an eccentric disk might be formed and sustained under precession with self-gravity. In BE00 N-body simulation, an inward bound $10^6 M_\odot$ star cluster is completely disrupted by the tidal shear of a $10^7 M_\odot$ black hole, consequently forming a thick, eccentric, stellar system. The alternative scenario by BA01 involves a circular disk, already present in the bulge, that gets excited into an eccentric disk by a natural $m = 1$ perturbation. The excitation may either be caused by a passing giant molecular cloud or globular cluster, which can induce the lopsidedness in the disk (seen in Fig. 1) that persists for 7×10^7 years in their simulations. However, for the non-axisymmetric waves to develop, the disk needs to be thin. They furthered considered a model in which a black hole was shifted from the center of the potential, and another where its velocity was perturbed. Too many particles escaped in the simulations for them to be viable. The model proposed by Sambhus & Sridhar (2001) extends Tremaine's (1995) eccentric disk to simulate a larger disk mass ($2 \times 10^7 M_\odot$) which involves a shredding of $10^5 M_\odot$ globular cluster near the vicinity of the SBH. Subsequently, the cluster stars merge into a pre-existing disk of few $10^7 M_\odot$, orbiting the central black hole on both prograde and retrograde, quasi-periodic, loop orbits. The $m = 1$ instability which causes

the large eccentricity is induced by resonant response to the counter-rotating orbits. In this model, lopsidedness of the eccentric disk geometry is created in response to the presence of retrograde orbits. All three models roughly reproduce the double nucleus geometry and the dynamics, such as the offset in the velocity dispersion profile from P2 by $\approx 0\farcs2$, to varying degrees of accuracy. However, one important difference between BE00 and BA01 + SS01 scenarios is that the BE00 model requires the stellar cluster be much less massive than ($\lesssim 10\%$) the black hole so that it can be disrupted. By contrast, the BA01 and SS01 models are constructed to have a much larger disk, about $20\% - 40\%$ of the total central mass concentration. These two scenarios can be directly tested if a mass estimate of the disk can be robustly measured, and the uncertainty can be quantified. The ambiguity in the bulge decomposition is reflected in the available photometry of P1, which can significantly differ in brightness from different studies. Furthermore, thus far it is not clear how much of P2 is part of the bulge or the eccentric disk.

In addition to the eccentric disk, the bulge structure of M31 and how it fits into the developing picture of galaxy formation are interesting on their own merits. However, their studies have been complicated by the double nucleus. The steepness of galaxy nuclei and correlations with other structural parameters (e.g. Faber et al. 1997) reflect the manner by which bulges are formed. Numerical simulations show that black hole mergers can flatten galaxy cores by ejecting stars from the center (e.g. Ebisuzaki, Makino, & Okumura 1991; Nakano & Makino 1999; and Milosavljević & Merritt 2001). This scenario appears promising for explaining the correlation found between large bulges and low central surface brightness. In this paper, I study the detailed properties of the M31 bulge by decomposing optical images to provide new structural parameters. With detailed decomposition one can address the following issues: Are there subtle structures in the bulge that are not obvious in full light? What are the relative contributions of the bulge, P1, and P2 components? What are their shapes? What is the bulge profile and how sharply is it peaked? Finally, I discuss what the new photometry of P1 and P2 reveal about the two competing scenarios that explain the formation of the eccentric disk. Although some of these questions can be addressed from other data in previous studies, this new analysis provides a unique look at the double nucleus based on a more flexible range of assumptions than foregoing studies.

In the sections to follow, Section 2 discusses the data, Section 3 briefly describes the analysis algorithm used to deblend the bulge. Section 4 discusses the decomposition, followed by the environment of the bulge in Section 5. Section 6 compares the eccentric disk formation models. Conclusions follow in Section 7.

Throughout the discussion I assume that the distance to M31 is $D = 770$ kpc, following KB99. I also assume that the Galactic extinction is $A_{\rm V} = 0.24$ (Burstein & Heiles 1984), which is similar to $A_{\rm V} = 0.21$ determined by Schlegel et al. (1998). Kormendy (1988) and KB99 dynamical models also suggest that $M/L \approx 5.7$ for the bulge stars. This is similar to star formation models of Bell & de Jong (2001), from which one can derive $M/L \approx 6$ based on the $V - I$ color of the bulge.

2. DATA

I obtain V-band ($\approx F555W$) data (GO 5236, Westphal) from the *HST* archive, as well as the deconvolved version from T. Lauer. The two sets of images are used for different purposes. The deconvolved version has been trimmed to a smaller field of view (FOV) of $11\farcs8 \times 11\farcs8$. While ideal for studying the nucleus, there is not enough realty for measuring the bulge profile and its shape. Therefore I also create a mosaic image with a FOV of $150'' \times 150''$, with a missing echelon in the Planetary Camera (PC) quadrant. The net exposure time is 300s, which has sufficiently high signal-to-noise (S/N) to measure the bulge profile. In addition to the deconvolved and mosaic images, I create a dithered image of the PC chip (FOV = $35'' \times 35''$) by combining four exposures of 300 second images. This will be used later for comparisons with the deconvolved image.

3. TECHNIQUE

3.1. *Algorithm*

I use a general galaxy fitting program called GALFIT to do the 2-D decomposition. Detailed information on the software and how it is implemented are found in a companion paper by Peng, Ho, Impey, & Rix (2002), but here I describe it briefly. One of the design capabilities of GALFIT is to accurately decompose nearby galaxies that are highly resolved to study them closely and uncover or extract galaxy sub-structures, such as nuclear disks, bars, and double nuclei. To be highly flexible, GALFIT allows simultaneous fitting of standard function types such as Sérsic (1968), Gaussian, exponential, and Nuker. The program has the option to either convolve the models with the PSF to simulate the seeing, or not convolve if the image has already been deconvolved. The number of components to fit is not limited a priori. GALFIT minimizes χ^2 residuals using a down-hill gradient/parabolic expansion method called Levenberg-Marquardt (Press et al. 1997) by iteratively creating model images, convolving them with the PSF, and subtracting them from the data. Even though the gradient method is not as "smart" as alternative Simulated Annealing or Metropolis algorithms, it has the virtue of being fast. As an example, fitting 6 components with 41 free parameters over the entire 400×400 pixel image, while doing convolution, takes roughly one minute per iteration on a Pentium 450 MHz computer, and converges in $30 - 50$ iterations. Speed is desirable because the χ^2 topology of the fit is complex; to adequately explore it and find an optimal fit thus requires testing various model combinations and initial parameters.

The merit function to minimize is the χ^2, or in normalized form, $\chi^2_\nu = \chi^2/N_{\rm dof}$, defined as:

$$\chi^2_\nu = \frac{1}{N_{\rm dof}} \sum_{x=1}^{nx} \sum_{y=1}^{ny} \frac{({\rm flux}_{x,y} - {\rm model}_{x,y})^2}{\sigma^2_{x,y}}. \qquad (1)$$

where $\sigma_{x,y}$ is the uncertainty, or weight, at each pixel; $N_{\rm dof}$ is the degree of freedom; nx and ny are the dimensions of the image in x and y direction. ${\rm Model}_{x,y}$ is the sum of all the model components fitted.

Traditionally, 2-D models use purely elliptical azimuthal shapes, but most galaxies are somewhat disky or boxy depending on whether they are more rotationally or pressure

supported, respectively. GALFIT can fit them by replacing the ellipses with a shape of,

$$r = \left(|x|^{c+2} + \left| \frac{y}{q} \right|^{c+2} \right)^{\frac{1}{c+2}}, \quad (2)$$

which can be rotated to any position angle (PA). The component shape is boxy if $c > 0$, disky if $c < 0$, and pure ellipse when $c = 0$. This azimuthal function was motivated originally by Athanassoula et al. (1990) to characterize the shapes of galaxy bars. The parameter q is the axis ratio of each component.

In the radial direction, the 1-D Sérsic light profile is defined as,

$$\Sigma(r) = \Sigma_e \, \exp^{-\kappa\left[(\frac{r}{r_e})^{1/n}-1\right]} \quad (3)$$

where r_e is the effective radius of the galaxy, Σ_e is the surface brightness at r_e, n is the power-law index, and κ is coupled to n such that half of the total flux is within r_e. The original de Vaucouleurs (1948) profile is the special case with $n = 4$ and $\kappa = 7.67$. The usefulness of the Sérsic function is that it can fit a continuum of profiles ranging from a Gaussian, to exponential, to a de Vaucouleurs, by smoothly varying the exponent: $n = 0.5$ for a Gaussian, $n = 1$ for an exponential disk, and $n = 4$ for de Vaucouleurs. In GALFIT, the flux parameter that is fitted is the total magnitude, instead of Σ_e. The translation between the total magnitude of a component and Σ_e is given in Peng et al. (2002).

Bulges that are modeled with the Sérsic profile have flat cores, but most galaxies have profile rise that extend into the resolution limit (e.g. Lauer et al. 1995, Carollo et al. 1997, Rest et al. 2001, and Ravindranath et al 2001). A function which can describe many double power-law and core type galaxy bulges in 1-D was introduced by Lauer et al. (1995), known as the Nuker law:

$$I(r) = I_b \, 2^{\frac{\beta-\gamma}{\alpha}} \left(\frac{r}{r_b} \right)^{-\gamma} \left[1 + \left(\frac{r}{r_b} \right)^{\alpha} \right]^{\frac{\gamma-\beta}{\alpha}} \quad (4)$$

There are five adjustable profile shape parameters: I_b, r_b, α, β, and γ. Taken to the limits of large and small radii, the parameter γ is the slope of the inner power law, and β is the slope of the outer power law. The break radius r_b is the location where the profile changes slope, I_b is the surface brightness at r_b, and α describes how sharply the two power laws connect. GALFIT fits the surface brightness magnitude μ_b instead of the intensity I_b. I generalize this profile to 2-D, hence there are 5 additional parameters: x_{cent}, y_{cent}, q, PA, and c.

To account for the PSF seeing when fitting models to the dithered image, GALFIT convolves a doubly oversampled PSF, created using Tiny Tim (Krist & Hook 1997), with the models. The Tiny Tim software can reproduce the core of WFPC2 PSFs well, even if the diffraction spikes are harder to reproduce. For convolution purposes this should suffice. Later in the paper, I will compare these results with fits to the deconvolved image of L98.

3.2. *Noise Image and Parameter Uncertainty Estimates*

Locally, the bigger of the two contributors to the root-mean-square (RMS) fluctuation of the data image is the surface brightness fluctuations (SBF) of star clusters resolved by the *HST*, rather than the Poisson noise. Unlike Poisson noise where the noise-to-signal ratio decreases as $\sqrt{\text{time}}$, the ratio of the SBF noise to the galaxy background asymptotically approaches a constant value. Thus, in this regime, the derived uncertainties in the fitting parameters remains constant with increasing exposure time. Moreover, while the Poisson noise correlates on scale of $\lesssim 1$ pixel in the dithered image, the SBF noise correlates on scales of a few pixels. To get realistic error bars from model fits thus requires having a reasonable estimate of the pixel weights, $\sigma_{x,y}$, that account for the SBF in a steeply rising galaxy bulge.

A Poisson map of the image bears an imprint of the SBF variance because the same star clusters that produce the Poisson signal are responsible for the SBF. I assume that the SBF RMS can be approximated by a scaling of the Poisson noise. To do so, I compute the ratio of the total RMS to the Poisson noise in 30×30 pixel boxes sampled randomly around the bulge in the dithered image. Then, multiplying this factor (1.9) to the Poisson map of the image, I obtain an approximate SBF noise image to use as pixel weights. The exact scale factor does not affect the estimated uncertainties because they are renormalized by $\sqrt{\chi^2_\nu}$ (see below). This scale factor appears reasonable, and for visually good fits, χ^2_ν comes out close to unity.

It is worth noting that the intrinsic galaxy SBF amplitude is higher than in the observed image because of PSF convolution. Moreover, because the SBFs are spatially resolved, PSF smearing correlates the SBF noise so that the pixels are not statistically independent. However, in scaling the pixel weights as described, the PSF correlation of the SBF is implicitly taken into account in the χ^2_ν statistics. To first order, the PSF smearing effectively reduces the $N_{\rm dof}$ in the observed image by a factor C. This factor is $C \sim \text{var}_{int}/\text{var}_{obs}$, where var_{int} is the intrinsic variance (i.e. without PSF filtering) and var_{obs} the observed variance (i.e. PSF-filtered). Furthermore, the effective pixel weights $\sigma^2_{x,y}$ have the same factor C, which cancels out of Equation [1] in calculating χ^2_ν.

Once GALFIT converges on a solution, it estimates the fitting uncertainties by using the covariance matrix of the parameters. For a more detailed discussion, see Peng et al. (2002), but here I give a brief description. Since χ^2 is a function of the fitting parameters, the surface of constant $\Delta\chi^2$ centered around the best fit χ^2_{min} can be roughly approximated as an n-dimensional ellipsoid, where n is the number of free parameters in the fit. Defined as the local χ^2 curvature with respect to all pairs of parameter combinations a_i and a_j, i.e. $\mathrm{d}^2\chi^2/(\mathrm{d}a_i\,\mathrm{d}a_j)$, the covariance matrix of the fit provides a handle on the correlation between parameters. To estimate parameter uncertainties accounting for correlation, I consider an ellipsoid which encloses a region up to $\Delta\chi^2 = 1$, which is the 68% confidence region for a single degree of freedom. The ellipsoid semi-major axes and their lengths are calculated from the eigenvectors and eigenvalues of the covariance matrix. I determine the uncertainty σa_i for parameter a_i by projecting the vector sum of all the major axes vectors onto the unit coordinate axis $\hat{a}_i$. In cases when the fit does not

produce a reduced $\chi^2_\nu \approx 1$, I also scale the uncertainties by $\sqrt{\chi^2_\nu}$ to avoid under-estimating them. Strictly speaking, while this method of estimating uncertainties is fair, it may produce uncertainties that are equal to or greater than the true uncertainties. This over-estimate is probably not a serious concern because, ultimately, the limitation is that we do not know how well the local χ^2 topology may be represented by an ellipse. Furthermore, the parameter values may not be normally distributed around the mean.

In the discussions to follow, I quote χ^2_ν and parameter values based on fits to dithered images rather than deconvolved images. Although the image of M31, with a very high S/N, has been deconvolved accurately, the process introduces an additional correlation by the PSF, which is hard to interpret in the presence of SBF. In comparison, the noise property of the unrestored image is easier to interpret. While the signal in individual, unrestored, images are correlated by the PSF from pixel to pixel, the Poisson noise is *uncorrelated*. Combining dithered images introduces at most a sub-pixel correlation which is small compared to the SBF. The correlation in the signal is accounted for in the fitting process by convolving the models with the PSF.

4. DECOMPOSITION

My attempt at decomposing the double nucleus is not the first of its kind, but is motivated by previous studies of L93, K95, and BA01, who perform 2-D image decomposition using iterative techniques. K95 fit the U-band image by first subtracting a smooth model of P2 from the data. Then, fitting isophotes to P1 and obtaining a smooth model, they use it to get a better estimate of P2. The process is then repeated. BA01 decompose the WFPC2 I-band image by assuming the bulge can be fitted by three Gaussians after masking out the central $2''$ of the image. In so doing, there is an implicit assumption that the galaxy core flattens out. The fit is then applied to V and U-band images after proper normalization. L93 use a nonlinear least-squares routine to deblend the nuclear region simultaneously with two components, assuming that P2 is indistinguishable from the bulge. Each component is concentric, with otherwise arbitrary position, brightness, ellipticity, and position angle.

My procedure is similar to L93 study, but with a more general set of assumptions: I relax the restriction that P1 and P2 are symmetric, and the number of components needed to fit them. The steepness of the bulge is a free parameter.

4.1. *Fitting Procedures*

4.1.1. *General Outline*

M31, being an Sb-type galaxy, has a large galactic disk component that spans 3.5° in diameter, with a bulge that has an effective radius of 4.′5 (KB99). Although the PC chip has twice the angular resolution to resolve the double nucleus compared to the Wide Field chips, the combined WFPC2 mosaic, with ≈ 3.′5 FOV, is better suited for measuring the large bulge. To take advantage of the capabilities of both PC and WFPC2, I perform fitting in two separate steps.

First I fit the bulge with a Nuker profile using the entire V-band mosaic image. To do so, I mask out the echelon-shaped region outside the PC, the dust lanes in the mosaic image, as well as inner $3''$ of the nucleus. Masking the nucleus does not seriously bias the bulge measurement because, in the second step, I take the fitted parameters for the bulge, and optimize it simultaneously along with other components for the nucleus in the PC chip. In this step the bulge position and inner slope parameter, γ, can vary freely, but all other *bulge* parameters are fixed at their optimal values. All the other *nuclear* components can change freely without constraints. The results are discussed in § 4.3, and summarized in Table 1. As an independent check on the decomposition, I perform a similar fit by replacing the Nuker bulge with a Sérsic bulge, presented in § 4.4.

I note that even though M31 has a large disk component, using 1-D decomposition, KB99 show that the extrapolation of the disk into the center, and within the WFPC2 FOV, is nearly constant at $\mu_V \approx 20.4$ mag/arcsec^2. Henceforth I adopt this value as a sky level in all fits.

4.1.2. *Determining the Number of Components*

I determine the number of components to fit iteratively by starting with the bare-minimum assumption, then increase that number to see how the fit improves χ^2. L93 has already found that two components failed to fit the M31 nucleus. Therefore, my first trial starts with three, representing P1, P2, and a bulge. For a three component fit, the χ^2_ν is 1.57, with $N_{\rm dof} = 1.6 \times 10^5$. In comparison, an excellent fit to the bulge in the PC image, after masking out the double nucleus, produces a significantly lower $\chi^2_\nu = 1.25$. The reason for the bad fit is that P1 is asymmetric (L93, K95, L98, and BA01), moreover, the UV peak is not centered on P2 (BA01). This can be gleaned from Figure 1 where the bright UV peak is displaced to slightly south-east of P2, and P1 is not purely ellipsoidal. To model asymmetry, each nucleus requires at least another component nearby, totaling five. I use the Sérsic profiles for most components, except for the bulge. For the bulge, I choose from either a Sérsic or Nuker component.

Fitting five components to just the PC image and not the mosaic, allowing *all* parameter to optimize (40-42 parameters, depending on whether a Sérsic or Nuker function is used), one can obtain a good fit with a $\chi^2_\nu = 1.31$. A closer examination reveals that the dominant component, i.e. the bulge, in this trial has an axis ratio $q = 0.90$ with uncertainty < 0.01. The fit might initially be deemed acceptable except for the fact that the bulge is noticeably elliptical in the mosaic image, with an axis ratio $q \approx 0.80$, and the inner nucleus is even more flattened. Therefore, at an intermediate radius, there must be a round component that dominates, and has significantly different properties than the larger scale bulge. I can derive meaningful bulge parameters from the mosaic image as described previously in § 4.1.1, and apply it fixed just to the PC image alone, using five components. Here again, the component with $q \geq 0.9$ reappears at a highly significant level, at the expense of the UV peak component. Inevitably, in a realization using five components, the UV peak is poorly fitted because it makes up only 0.1%, compared to the round bulge component, which makes up as much as 16%, of the flux in the inner few arcseconds. The round $q \geq 0.9$ com-

ponent can in principle be a stellar disk seen face on, but this is unlikely. It has a half light radius 2.″4 to 3″, roughly five times the double nucleus separation. Hence, from here on I group this component with that of the bulge, but designate it as the "spherical" bulge (fifth component in Table 1) to distinguish from the large scale bulge component. I will return to a more detailed discussion of the spherical component in Section 4.6.

The best fit, therefore, requires six components, with $\chi^2_\nu = 1.30$: two for each nucleus, and two bulge-like components, to be discussed shortly. To fit P1 and P2, Sérsic models do a fine job without having to use a more flexible Nuker function. Table 1 summarizes the properties of all the components for two different trials. In the first trial, I fit the dominant galaxy bulge with a 2-D Nuker model, and in the second, with a Sérsic model. I discuss these two scenarios with more detail independently in § 4.3 and § 4.4.

4.2. *Uniqueness and Meaning of the Components*

To fit the double nucleus accurately I ultimately resort to fitting the image with six components, with 40-43 free parameters, which might seem bewilderingly large and ill-constrained. I emphasize however, that they may not all be physically distinct components. In particular two components are used each for the bulge and P1 because they are not simple to parameterize. Therefore, it may be more meaningful to interpret the sum of each pair as a single component rather than each as separate entities.

With a high number of components, several issues can be raised regarding the uniqueness and validity of decompositions (A. Quillen and T. Lauer, private communication). First, if the nuclei are related to an eccentric disk, its light distribution may be irregular and may not be parameterizable. So even if the decomposition may look acceptable, the model will not be physically meaningful. Another objection is that the presence of the disk may perturb the bulge enough kinematically to invalidate the assumption that the bulge is smooth at the center. Therefore, extrapolating the bulge profile into the center based on outer regions may be unreliable.

I argue that there is evidence that the bulge profile is not disrupted much by the process of the double nucleus formation: Often, kinematics can reveal subtle physical attributes (e.g. kinematically decoupled core) that are not obvious in the starlight. Published rotation curves and velocity contours show that the nucleus has a regular solid body rotation out to 0.″5, which becomes Keplerian beyond 1″ (KB99, BA01). The kinematic curves are otherwise featureless apart from the velocity dispersion peak being offset 0.″2 from the UV peak away from P1. Therefore, either the formation of the disk has not been sufficiently violent to disarrange the nuclear dynamics, or the perturbations have relaxed into the bulge. Hence I believe the bulge can be parameterized by smooth functions down to small physical scales. Furthermore, I believe that the degree to which the double nucleus is parameterizable and regular may yield insights into the eccentric disk and formation model predictions on the morphology. Being a complicated system, irregularities in the nuclei would likely show up in the residuals because the functions I fit have a high degree of symmetry. Recognizing, however, that inferences about the morphology of the double nucleus is intimately tied to the bulge, I will check how assumptions about the bulge can affect the decomposition. As a prelude to discussions to come, I find that, throughout various trials for the bulge, the sum of the parts for P1, P2, and the bulge, result in fundamentally similar components, even if individual sub-components may not be unique. For these reasons I believe the decomposition to be valid and robust. But ultimately, as with K95 I let the smoothness and the pattern of the residuals be an empirical guide to what is a reasonable solution.

4.3. *Nuker Bulge*

In their fit to a 1-D bulge profile, KB99 obtain the Nuker parameters: $\mu_b = 17.55 \pm 0.66$, $r_b = 67.''7 \pm 62.''1$, $\alpha = 1.08 \pm 0.59$, $\beta = 1.51 \pm 0.57$, $\gamma = 0.25 \pm 0.25$, based on a fit to a region $5.''5 \leq r \leq 300''$, excluding the double nucleus. The large uncertainties are due to parameter coupling in the Nuker profile. As initial parameters to my fit of the bulge, I use the values from KB99 but allow them to vary.

The best fit model I obtain, according to χ^2, has a bulge that is represented by a Nuker model, with an overall $\chi^2_\nu = 1.30$. In all, six components are used, and they fit the entire bulge region well, as shown in Figure 2. Figure 2b shows the net residuals; Fig. 2c shows the model + residual for P1, and similarly for P2 in Fig. 2d. The images shown in Fig. 2 are fits to deconvolution restored image of L98, but the numbers presented in Table 1, including χ^2_ν are from the unrestored image for reasons in § 3.2. In comparison to KB99, my fits to the mosaic and dithered PC images produce parameters very similar to that obtained by KB99, to within their uncertainties: $\mu_b = 17.76$, $r_b = 66.''48$, $\alpha = 1.10$, $\beta = 1.99$, $\gamma = 0.17$. My central cusp measurement, $\gamma = 0.17$, is slightly shallower than KB99, $\gamma = 0.25$, in this more detailed fit to the double nucleus.

In this model, the centroid of the bulge component is displaced from the UV peak, by $(\Delta\mathrm{RA}, \Delta\mathrm{DEC}) = (-0.''06, -0.''15)$, which is a direction away from the dust patches in the bulge. Such a large shift is most likely due to disturbance by dust around the nucleus; forcing the bulge to be centered on the UV peak increases the χ^2_ν by 0.003. In light of the unknown effect by dust, this small difference may not be statistically significant.

The residual error in Fig. 2b is 6% on average at the location of the worst fit, which is comparable to the SBF. The parameters obtained using the dithered and deconvolved images agree very well to within the uncertainties. Figure 3 shows the residuals near the double nucleus divided by the RMS image – the calculation of which was discussed in § 3.2. The worst fit within the 1″ circle is near P1 at $(-0.''22,\ 0.''04)$, where one pixel deviates by $-3.7\times$RMS. Indeed, even though the fit is overall quite good, there are differences between the model and the data. In Figure 4, I show the model image by summing P2 (without the UV peak) and the two components of P1, together making up the eccentric disk. The contour spacing is 0.1 magnitude and the circle at (0″,0″) marks the location of the UV peak. Comparing Fig. 4 and Fig. 1 shows that although the asymmetry of P1 is well modeled, P1 in the data is slightly rounder than the model, causing an oversubtraction near $(-0.''22,\ 0.''04)$. Simultaneously fitting a

7th component to the image does reduce the ellipticity of P1 somewhat, and reduces the χ^2_ν by 0.02. However, as the superficial improvement does not affect the results below, I choose to present a simpler model using 6 components.

The major axis orientation of the eccentric disk shown in Fig. 4 is at PA=59.25°. Assuming the disk is thin and circular at outer isophotes, its inclination is $50 \pm 1°$ to our line of sight. The sum of the fluxes from P1+P2 is $m_{\rm v} = 13.12 \pm 0.06$, or $M_{\rm v} = -11.55$ after correcting for galactic extinction and distance. The mass of P1+P2 is $M_{\rm P1+P2} = 2.1 \times 10^7 M_\odot$. In isolation, P1 has a brightness of $m_{\rm v} = 13.65$ mag.

Figure 5 shows the radial surface brightness profile of the components resulting from the decomposition (shifted to a common center), as well as shape parameters from isophote fitting the entire WFPC2 mosaic *V*-band image. In that figure, I represent the individual components used in the fit as dashed lines. Because P1 is asymmetric, I only show the brighter of the two sub-component, P1a. The UV peak is not plotted. The solid data points shown with errorbars are the intrinsic profile of the bulge in the absence of the double nucleus. Exterior to $5''$, those points are measured from isophote fits to the raw image, but interior, they have to be extrapolated from the analytic model fits because of the double nucleus. To do so, I create an image of the bulge by summing the Nuker and spherical bulge components, then fit it with isophotes. For completeness, I also show the shape parameters of the bulge out to $100''$; the *cos* 4θ panel is a measure of the diskiness (> 0) and boxiness (< 0) of a given isophote. The bulge is only slightly boxy, evidenced in cos4θ and from 2-D fits ($c = 0.05$). The presence of the spherical bulge component is manifest in the dip in the ellipticity profile at $r = 2''$. Although the bulge profile in general appears to be smooth with a gentle curvature farther out, with no apparent breaks (see KB99), in the decomposition, there appears to be a break at a radius of $1\farcs91$. This kind of behavior is sometimes seen in large bulges or spheroidal systems (e.g. Lauer et al. 1995, Peng et al. 2002). I plot a 1-D Nuker function having the parameters shown in the figure to guide the eye; it is not strictly a fit that minimizes the χ^2. I will discuss this break in more detail in § 5.

For the remainder of this sub-section, I test the extent to which P1 and P2 are affected by details of the bulge decomposition. To put a limit on the central cusp of the bulge I remove the UV peak model and instead fit the bulge to that location and allow all the parameters to re-optimize. The profile of the UV peak differs significantly from that of the bulge, and the χ^2_ν increases by ~ 0.01 to 1.31, with $\gamma = 0.19$.

In this model, the bulge component is centered on the UV peak. However, P2 remains significantly off-centered from the UV peak by $(\Delta{\rm RA}, \Delta{\rm DEC}) = (-0\farcs24, -0\farcs15)$. I test to see if this is real or is caused by fitting degeneracy by forcing P2 to the UV peak position. I refit both the deconvolved image of L98 and my own dithered image. Both fits produce residuals much worse than the asymmetric models. In particular, in the unrestored image the region in between P1 and P2 is significantly over-subtracted.

To constrain the luminosities of P1 and P2, hence the eccentric disk itself, I increase the nuclear slope parameter γ from the best fit value. If γ is forced up to 0.40, the fit significantly oversubtracts the bulge, which can be safely ruled out. This fit puts a lower limit on the brightness of P1 to be 0.15 mag, and P2 to be 0.4 mag, fainter than the optimal fit.

In their decomposition, K95 find that P1 has a brightness of $m_{\rm v} = 14.8$, and in L93, they find 14.5. My numbers are significantly brighter than both by about 0.9 to 1.2 magnitude. The differences may be in my assumptions about the true shape of P1 and P2, as well as the relative contribution of the bulge. L93 assume that both P1 and P2 are individually symmetric and concentric, with the bulge centered on P2. Part of the remaining differences might also be in the criteria of smoothness. My criterion is formally more strict than theirs. L98 also find the blue UV peak to have $m_{\rm v} = 18.7 \pm 0.3$, in good agreement to my finding of $m_{\rm v} = 19.07 \pm 0.52$, which is represented by a Sérsic profile. Both the large uncertainty and the large boxiness, $c = 0.67 \pm 0.02$, are caused by the SBF.

4.4. *Sérsic Bulge*

To test how different assumptions about the galaxy bulge can affect the decomposition of P1 and P2, I redo the above fit by replacing the Nuker bulge component with a Sérsic model. Figure 6 shows the surface brightness profile and shape parameter plots similar to Figure 5. The most prominent difference between the two is the extent of the bulge profile slope inner to a radius of $\approx 2''$. In terms of χ^2_ν, this fit is degenerate with that presented in Figure 5.

Another notable difference between this decomposition and the previous is the strength of the spherical bulge component, which now has a brightness of $m_{\rm v} = 13.51$. Although this component is somewhat fainter than the previous fit ($m_{\rm v} = 12.76$), it is still a significant component in the bulge relative to P1 and P2.

In this realization, the light from the two components P1 and P2 adds up to $m_{\rm v} = 13.06$, which is nearly identical to the nominal fit with a Nuker bulge above. P1 has a magnitude $m_{\rm v} = 13.66$, again, nearly identical to before. This decomposition illustrates the main point of these different exercises – that throughout various trials, although the sub-components of P1 or P2, and even the bulge contribution, may not be unique, their summed flux values and shapes are insensitive to model assumptions and initial parameter values. In the discussions below, I formally adopt the parameters from the Nuker bulge decomposition because it gives a slightly better fit statistically, and is a more general fit to the bulge, whereas the Sérsic profile has, by definition, a flat core.

4.5. *The Spherical Bulge Component*

In the previous two sub-sections, I preluded the presence of an underlying spherical component embedded inside a much larger bulge, and is distinct from the double nucleus. With the bulge accurately removed, this extra component has an axis ratio $q = 0.97 \pm 0.02$, an effective radius of 12 pc ($3\farcs2$), and close to an exponential disk profile. In comparison, the bulge has an axis ratio of $q = 0.81 \pm 0.01$. The spherical component half light radius is roughly 5 times the separation of the double nucleus, moreover, contains 16% of the flux within $2''$ (Table 1). It is essential for a good fit, both qualitatively and quantitatively, as shown

throughout various trials above.

The spherical bulge component is not likely to be caused by dust in the bulge. Figure 7 shows a bulge subtracted residual map of the entire WFPC2 mosaic in the *V*-band. Superimposed on the residual map are contours from the image prior to subtraction. The compass arrows show the major axis orientation of the large-scale galactic disk and bulge. Apparently, the bulge isophotes are elliptical well into the central few arcseconds, where there is little sign of dust. In fact, Figure 8 shows a $V-I$ color map of the WFPC2 FOV, revealing strong color differences in areas affected by dust. Remarkably, within $10''$ of the center, the presence of dust actually diminishes. Rather than due to dust, the existence of the spherical component most likely results from a small but significant departure from the Nuker profile and shape of the bulge.

Quillen, Bower, & Stritzinger (2000), using *HST* NICMOS images, discover that many galaxies, especially luminous core-types with boxy isophotes, have rounder isophotes at small radii. Peng et al. (2002) also show that a spherical component can be accurately extracted from the centers of some other galaxies. There are two theoretical models that predict the decrease in ellipticity and boxiness. One involves the mixing of stochastic orbits by the presence and growth of the central SBH (Norman, May, & van Albada 1985; Gerhard & Binney 1985; and Merritt & Valuri 1996), which steepens the central cusp. The other involves a dissipationless merging of binary black holes that scatter stars from the center (Milosavljevic & Merritt 2001), thereby flattening the nuclear cusp, with a break radius that can extend well beyond the sphere of influence of the SBH. In Milosavljevic & Merritt (2001) model, binary black holes of similar mass can eject stars amounting to the combined mass of the black holes. Consequently, these randomized stellar orbits, after redistributing in phase space, could conceivably have produced a spherical bulge component, whose mass would then be roughly that of the coalesced black holes. The discovery of the spherical component, in addition to the shallowness of the bulge cusp, suggest that the binary merger scenario is a more natural explanation for the bulge formation. Furthermore, the mass of the spherical component inferred from its luminosity of $m_{\rm v}=12.76$ is $2.8\times10^7 M_\odot$ – a mass surprisingly similar to the SBH of $3\times10^7 M_\odot$. It remains to be seen whether this agreement is a mere coincidence, or a confirmation that the bulge had been scoured by merging binary black holes.

If the spherical bulge component resulted from a binary black hole merger scenario, then the eccentric disk was formed more recently than the bulge. The mixing of stellar orbits after a binary SBH merger would have erased any organized sub-structure that previously resided at the nucleus. This hypothesis is consistent with the finding of SBV98, who discover that the nuclear stars are significantly younger than stars in the bulge.

5. LARGE SCALE BULGE PROPERTIES

5.1. *Bulge Parameters and Correlations*

KB99 show a 1-D profile of the bulge, assembled piecewise from several studies, out to $6300''$. Their plot shows that the bulge has a gentle curvature which has no meaningful break radius. On the other hand, in my representations of Figures 5 and 6, the bulge appears to have a triple power law with a distinct break in the bulge profile near $2''$ which has not been seen before because of the complications caused by the double nucleus below $r=5''$. From § 4.3, I obtain 2-D Nuker parameters that are very similar to those obtained by KB99, which is seen as a dashed line in Figure 5, and which indeed does have a large break radius. However, including the spherical bulge reveals there to be a significant break at $r\approx2''$. Whereas before, inferring from the Nuker fit alone, M31 bulge falls outside of the correlation between r_b with galaxy luminosity and μ_b found by Faber et al. (1997), my bulge decomposition shows that the correlation now holds very well. My new estimates on the luminosity density (j), slope (γ), and the corresponding mass density (ρ), and slope (ψ) values are listed in Table 2. They, too, now fall within correlations with galaxy luminosity shown in Faber et al. (1997).

5.2. *Spiral Dust Structure and Color Gradient*

The decomposition of the mosaic *V*-band image (Figure 7) shows a beautiful dust lane that runs from the lower-left of the image towards, but stopping near, the center of the nucleus, and reappearing on the other side. This feature has previously been noted in ground based studies of Wirth, Smarr, & Bruno (1985) and SBV98. In SBV98, the spiral dust arms extend out to roughly $30''$ on both sides of the nucleus.

The color map of Figure 8 reveals a significant gradient between the nucleus and the bulge further out, toward the South. It also highlights the winding dust lanes towards the nucleus. However, it is curious that despite the extensive structure, the dust arms appear to stop within $10''$-$15''$ of the center. This will be discussed further in § 7. The color difference between the nucleus and its immediate surrounding noted by L98 and BA01 is evident.

6. FORMATION OF ECCENTRIC DISK BY NATURAL $m=1$ MODE VS. DISRUPTION

The mass of P1+P2 is instrumental for deciding between competing models that form the double nucleus, in particular between the natural $m=1$ models (BA01 and SS01), and the star cluster disruption model of BE00. All three produce an eccentric disk as proposed by Tremaine, and broadly satisfy key dynamical and morphological constraints. In BE00 model, the key requirement is that the globular cluster gets completely disrupted and scattered into a thick disk by the SBH. A massive cluster with strong self-gravity must approach the black hole at a low impact parameter, which translates into a disk with high ellipticity and a short life time. To satisfy the morphological and dynamical constraints, the cluster size is limited to $\lesssim 3\times10^6 M_\odot$. On the other hand, the BA01 and SS01 models can be considerably more massive, in the range $0.7\text{-}2.1\times10^7 M_\odot$.

My nominal integrated brightness for P1+P2 is $m_{\rm v}=13.12\pm0.06$ which translates to a mass $2.1\times10^7 M_\odot$. In comparison to globular clusters in M31 (Barmby, Huchra, & Brodie 2001), P1 alone ($m_{\rm v}=13.65$, $M=1.2\times10^7 M_\odot$) would at least be in the 90 percentile of the most luminous globular clusters. Table 1 lists two sets of masses for apertures $r=1''$ and $r=2''$ centered on the UV peak, for all the components. I find that within $r=1''$ of the UV peak,

the masses of the components are $M_{bulge} = 8.3 \times 10^6 M_\odot$, $M_{P1} = 7.4 \times 10^6 M_\odot$, and $M_{P2} = 5.0 \times 10^6 M_\odot$. The sum P1+P2 is comparable to the black hole mass of $3 \times 10^7 M_\odot$. For convenience, I also provide masses within $2''$ aperture of the UV peak in Table 1.

The total mass of P1+P2 determined here is about an order of magnitude too high for the globular cluster disruption scenario to work. I note that P1 alone has sufficient mass to rule out this scenario, if P2 is at least in part considered as the bulge. The eccentric disk masses determined by L93 and K95 can rule out the globular cluster disruption scenario, as well. BA01 also conclude the disk is massive, $1.7 \times 10^7 M_\odot$, based on modeling the bulge with multiple Gaussians. My mass determination for the eccentric disk, being higher than the first two studies, provides additional buffer to rule out reasonable uncertainties in the M/L ratio by factors of a few. On the other hand, my P1+P2 flux is somewhat fainter (by 0.57 mag) than the measurement of $m_{\rm v} = 12.55$ by KB99. All estimates of the disk mass are that it is massive, while Section 4 has shown that the uncertainty due to the bulge decomposition amounts to about 6%. Therefore, the formation model favored is that of BA01 or SS01. In their models, an initial circular disk of stars was formed in the bulge, but became more eccentric after a brief encounter with a giant molecular gas cloud or a globular cluster, which need not be disrupted.

The discovery of a spherical bulge component confirms that the bulge potential is spherical around the double nucleus, which might be important for sustaining a thin eccentric disk. In a triaxial potential, an uniformly precessing eccentric disk, held together by self-gravity, is subject to tidal torque exerted by the bulge, which can cause misalignments in the orbital configuration, or cause the orbits to diffuse into the bulge through phase mixing.

7. DISCUSSION AND CONCLUSION

I decompose M31 with GALFIT to accurately extract the double nucleus. The large scale bulge is made up of two components: a small, spherical structure, embedded at the center of a large, and moderately elliptical component. I then use the decomposition to study the structural parameters of the bulge, finding that the break radius, r_b, correlates with other galaxy parameters that are found in Faber et al. (1997) for a large sample of early-type galaxies. The spherical component extracted has a mass of $2.8 \times 10^7 M_\odot$, which is surprisingly similar to the mass of M31's supermassive black hole. It remains to be seen whether this is the result of binary black hole mergers, as predicted by Milosavljevic & Merritt (2001) N-body simulations, or a mere coincidence.

The inferred mass of P1 and P2 combined is comparable to the black hole mass, and the bulge mass contained in a small region out to the radius of $1''$ from UV peak, with relative masses $M_\bullet : M_{bulge} : P1 : P2 = 4.3 : 1.2 : 1 : 0.7$. The inferred mass of P1+P2 is insensitive to the bulge parameters, as others (e.g. BA01) had also found. Coupled with the large impact parameter suggested by the disk, it seems a cluster that resulted in the eccentric disk of P1+P2 ($M \approx 2.1 \times 10^7 M_\odot$) could not have been disrupted enough by the black hole ($M_\bullet \approx 3 \times 10^7 M_\odot$) to form an eccentric disk around it. In such a scenario, the progenitor of P1+P2 would have to be still larger than my mass estimate.

The large mass of the disk is consistent with a scenario in which a stellar disk was formed in the nucleus, then became more eccentric after an $m = 1$ perturbation, by, for example, passing giant molecular clouds or globular clusters (BA01). Another possibility is that an approaching globular cluster of mass $\lesssim 10^6 M_\odot$ might have come within, and was shredded by, the SBH, then was integrated into the pre-existing disk (SS01). Despite how well the current N-body simulations reproduce the kinematics and morphologies, given that all the components within $2''$ of the bulge are comparable in mass, a perturbation that would excite the $m = 1$ mode in the disk might also perturb the bulge. Thus it is unclear whether their mutual tidal interactions need to be further considered in N-body simulations, or might a smooth bulge potential suffice.

The N-body simulations, coupled with a hypothetical shroud of dust at the nucleus, might explain both the eccentric disk geometry as well as the slight color difference between the bulge and the nucleus. However, it can not be the whole story: KB99 show that P1 and P2 have metal line strengths stronger than any globular cluster, hence they are unlikely to be the digested remnant of a globular cluster or an elliptical galaxy. A more complete picture also needs to account for the differing bulge and nuclear stellar ages inferred by SBV98. One viable scenario as suggested by L98 is that the disk formation was a separate event that occurred well after the formation of the bulge. This may be the case because the bulge formation event would have disrupted any pre-existing sub-structure at the center. To grow a disk to $2.1 \times 10^7 M_\odot$, one scenario is by the disruption of several globular clusters. However, this possibility is remote because angular momentum conservation and scattering by the SBH would tend to produce a more spheroidal geometry. A more likely explanation, in private communication with L. C. Ho, is that a significant amount of gas and dust roughly $2.1 \times 10^7 M_\odot$ had accreted into the center. Indeed, extended dust structures in Figures 7 and 8, as well as SBV98, strongly suggest it was a possibility. Through gravitational settling, a circular gas+dust disk enriched with reprocessed material could have grown steadily, out of which young stars would then form. This might explain the metallicity enhancement and the younger stellar population in the nucleus compared to the bulge. The disk might have subsequently experienced a kick from a passing GMC or a globular cluster that increased the eccentricity.

However, it is unclear at the moment how long ago or how such a massive $2.1 \times 10^7 M_\odot$ disk could have settled into the center. Assuming that the accretion occurred in the form of gas, the rate is limited by the near absence of non-thermal AGN activity at the M31 nucleus. Perhaps a significant amount of wind from star formation near the center might quench the AGN activity by blowing fuel away from the central engine (C. D. Impey, private communication). The accretion + wind scenario is attractive for explaining the possible presence of a UV star cluster at the center, and for the absence of dust lanes in the immediate vicinity of the double nucleus, despite there being a large and extended dust structure mere $20''$ away (Figs. 7 and 8).

Acknowledgments. I thank Peter Strittmatter for financial support. I also thank Luis Ho and Chris Impey for comments and reading the original draft; Alice Quillen, and Dennis Zaritsky, and Roelof de Jong, for general discussions; Daniel Eisenstein for assistance in the error propagation; and Tod Lauer for providing the deconvolved images of M31, and for discussions about the SBF and fitting of the double nucleus. I also thank the referee for helpful and insightful comments. This research has made use of the NASA/IPAC Extragalactic Database (NED) which is operated by the Jet Propulsion Laboratory, California Institute of Technology, under contract with the National Aeronautics and Space Administration.

REFERENCES

Andredakis, Y. C., & Sanders, R. H. 1994, MNRAS, 267, 283
Athanassoula, E., Morin, S., Wozniak, H., Puy, D., Pierce, M. J., Lombard, J., & Bosma, A. 1990, MNRAS, 245, 130
Bacon, R., Emsellem, E., Combes, F., Copin, Y., Monnet, G., & Martin, P. 2001, A&A, 371, 409 [BA01]
Barmby, P., Huchra, J. P., & Brodie, J. P. 2001, ApJ, 121, 1482
Bekki, K. 2000, ApJ, 540, L79. [BE00]
Bell, E. F., & de Jong, R. S. 2001, ApJ, 550, 212
Burstein, D., & Heiles, C. 1984, ApJS, 54, 33
Burstein, D., Bertola, F., Buson, L. M., Faber, S. M.,& Lauer, T. R. 1988, ApJ, 328, 440
Carollo, C. M., Stiavelli, M., de Zeeuw, P. T., & Mack, J. 1997, AJ, 114, 2366
Corbin, M. R., O'Neil, E., & Rieke, M. J. 2001, AJ, 121, 2549
de Vaucouleurs, G. 1948, Ann. d'Astrophys., 11, 247
Dressler, A., & Richstone, D. O. 1988, ApJ, 324, 701
Ebisuzaki, T Makino, J., & Okumura, S. K. 1991, Nature, 354, 212
Emsellem, E., & Combes, F. 1997, A&A, 323, 674
Faber, S. M., Tremaine, S., Ajhar, E. A., Byun, Y.-I., Dressler, A., Gebhardt, K., Grillmair, C., Kormendy, J., Lauer, T. R., Richstone, D. 1997, AJ, 114, 1771
Garcia, M. R., Murray, S., S., Primini, F. A., Forman, W. R., McClintock, J. E., & Jones, C. 20000, ApJ, 537, 23
Gerhard, O. E., & Binney, J. 1985, MNRAS, 216, 467
Jalai, M. A., & Rafiee, A. R. 2001, MNRAS, 320, 379
King, I. R., Stanford, S. A., & Crane, P. 1995, AJ, 109, 164. [K95]
Kormendy, J. 1987, in IAU Symp. 127, Structure and Dynamics of Elliptical Galaxies, ed. T. de Zeeuw (Dordrecht:Reidel), 17
——. 1988, ApJ, 325, 128
Kormendy, J., & Bender, R. 1999, ApJ, 522, 772. [KB99]
Krist, J., & Hook, R. 1999, The Tiny Tim User's Guide (Baltimore: STScI)
Lauer, T. R., Faber, S. M., Groth, E. J., Shaya, E. J., Campbell, B., Code, A., Currie, D. G., Baum, W. A., Ewald, S. P., Hester, J. J., Holtzman, J. A., Kristian, J., Light, R. M., Lynds, C. R., O'neil, & E. J. Jr. 1993, AJ, 106, 1436. [L93]
Lauer, T. R., Ajhar, E. A., Byun, Y.-I., Dressler, A., Faber, S. M., Grillmair, C., Kormendy, J., Richstone, D., & Tremaine, S. 1995, AJ, 110, 2622
Lauer, T. R., Tremaine, S., Ajhar, E. A., Bender, R., Dressler, A., Faber, S. M., Gebhardt, K., Grillmair, C. J., Kormendy, J., & Richstone, D. ApJ, 1996, 471, 79
Lauer, T. R., Faber, S. M., Ajhar, E. A., Grillmair, C. J., & Scowen, P. A. 1998, AJ, 116, 2263. [L98]
Light, E. S., Danielson, R. E., & Schwarzschild, M. 1974, ApJ, 194, 257
Merritt, D., & Valuri, M. 1996, ApJ, 471, 82
Milosavljević, M. & Merritt, D., 2001, ApJ, 563, 34
Mould, J., Graham, J., Matthews, K., Soifer, B. T., & Phinney, E. S., 1989, ApJ, 339, L21
Nakano, T., & Makino, J. 1999, ApJ, 510, 155
Nieto, J. -L., Macchetto, F. D., Perryman, M. A. C., di Serego Alighieri, S., & Leliévre, G. 1986, A&A, 165, 189
Norman, C. A., May, A., & van Albada, T. S. 1985, ApJ, 296, 20
Peng, C. Y., Ho, L. C., Impey, C. D., Rix, H.-W. 2002, AJ submitted.
Press, W. H., Teukolsky, S. A., Vetterling, W. T., & Flannery, B. P. (1992). Numerical Recipes in C, Cambridge University Press
Quillen, A. C., Bower, G. A., & Stritzinger, M. 2000, ApJ, 128, 85
Quillen, A. C., McDonald, C., Alonso-Herrero, A., Lee, A., Shaked, S., Rieke, M. J., & Rieke, G. H. 2001, ApJ, 547, 129
Ravindranath, S., Ho, L. C., Peng, C. Y., Filippenko, A. V., & Sargent, W. L. W. 2001, AJ, 122, 653
Rest, A., van den Bosch, F. C., Jaffe, W., Tran, H., Tsvetanov, Z., Ford, H. C., Davies, J., & Schafer, J. 2001, AJ, 121, 2431
Richstone, D., Bower, G, & Dressler, A. 1990, ApJ, 353, 118
Salow, R. M., & Statler, T. S. 2001, ApJ, 551, L49. [S99]
Sambhus, N., & Sridhar, S. 2001, astro-ph/0110274
Schlegel, D. J., Finkbeiner, D. P., Davis, M. 1998, ApJ, 500 525
Sérsic, J. L. 1968, Atlas de Galaxias Australes (Cordoba: Observatorio Astronomica)
Sil'chenko, O. K., Burenkov, A. N., & Vlasyuk, V. V. 1998, A&A, 337, 349 [SBV98]
Statler, T. S., King, I. R., Crane, P., & Jedrzejewski, R. 1999, AJ, 117, 894
Tremaine, S 1995, AJ, 110, 628
Wirth, A., Smarr, L. L., Bruno, T. L. 1985, ApJ, 290, 140

TABLE 1
TWO DIMENSIONAL IMAGE FITTING PARAMETERS

Trial $m_v(r \leq 1'' \ \& \ 2'')$ Mass($r \leq 1'' \ \& \ 2''$)	Func.	$\Delta\alpha$ ($''$)	$\Delta\delta$ ($''$)	f/f_{tot} r$\leq 1''$	f/f_{tot} r$\leq 2''$	m_v, μ_v (mag)	$r_{b,e}$ ($''$)	α, n	β	γ	a/b	PA (deg)	c	χ^2_ν	Comments
(1)	(2)	(3)	(4)	(5)	(6)	(7)	(8)	(9)	(10)	(11)	(12)	(13)	(14)	(15)	(16)
Solution 1:	Sérsic	$\equiv 0.$	$\equiv 0.$	0.004	0.002	19.07	0.08	0.42			0.63	70.4	0.67	1.30	UV peak
Nuker bulge	Sérsic	-0.24	-0.15	0.24	0.15	14.17	0.87	0.98			0.66	54.3	0.05		P2
	Sérsic	0.31	0.42	0.26	0.16	13.88	1.00	1.31			0.62	64.8	-0.24		P1a
13.10, 12.20 mag	Sérsic	0.49	0.37	0.08	0.05	15.46	0.37	0.69			0.92	-46.8	0.57		P1b
	Sérsic	0.13	-0.06	0.11	0.16	12.76	3.21	0.83			0.97	56.0	0.14		Spherical bulge
$2.07 \times 10^7 M_\odot$,	Nuker	-0.06	-0.15	0.29	0.45	17.76	66.48	1.10	1.99	0.17	0.81	50.1	0.05		Bulge
$4.75 \times 10^7 M_\odot$	Offset			0.01	0.01	20.4									mag/arcsec^2
Solution 2:	Sérsic	$\equiv 0.$	$\equiv 0.$	0.005	0.002	18.86	0.09	0.41			0.67	60.7	1.99	1.30	UV peak
Sérsic bulge	Sérsic	-0.22	-0.14	0.27	0.18	13.98	0.90	1.00			0.69	55.6	0.01		P2
	Sérsic	0.33	0.43	0.28	0.20	13.83	0.90	1.20			0.66	64.9	-0.26		P1a
13.10, 12.20 mag	Sérsic	0.51	0.38	0.07	0.04	15.77	0.36	0.68			0.88	-44.7	0.83		P1b
	Sérsic	0.00	0.16	0.08	0.11	13.51	2.40	0.44			0.96	56.6	0.08		Spherical bulge
$2.07 \times 10^7 M_\odot$,	Sérsic	0.10	-0.17	0.29	0.47	4.97	214.71	2.00			0.81	52.0	0.06		Bulge
$4.75 \times 10^7 M_\odot$	Offset			0.01	0.01	20.4									mag/arcsec^2
Uncertainties		0.02	0.02			0.2	2%	0.03	0.02	0.02	0.03	2	0.02		

Note. — Col. (1): Fitting trials for Nuker or Sérsic bulge type, apparent visual magnitude within an aperture $1''$ and $2''$ radius centered on the UV peak, and the corresponding inferred *luminous* mass based on $M/L = 5.7$. Col. (2): Galaxy components used in the fit. Col. (3): RA offset. Col. (4): DEC offset. Col. (5): The fraction of component flux with respect to the total integrated flux (Col. 1), all within a $r = 1''$ aperture centered on the UV peak. Col. (6): Same as Col. 5, but with $r = 2''$ aperture. Col. (7): For Nuker, it is the surface brightness at the breaking radius. For the Sérsic profile it is the total brightness. For the *offset* component (which represents an exponential disk) it is the surface brightness magnitude. The magnitudes are not corrected for galactic extinction. Col. (8): r_b is the breaking radius for the Nuker power law, r_e is the effective radius of the Sérsic law. Both have units in arcseconds. Col. (9): For Nuker, α parameterizes the sharpness of the break. For Sérsic, n is the Sérsic exponent $1/n$. Col. (10): Nuker asymptotic outer power law slope. Col. (11): Nuker asymptotic inner power law slope. Col. (12): Axis ratio. Col. (13): Position Angle. Col. (14): Diskiness (negative)/boxiness (positive) parameter. Col. (15): Reduced χ^2 of the fit. Col. (16): Comments: P1a and P1b add to form a single component P1. The last row shows the "representative" uncertainties for the ensemble of profiles. Individual uncertainties are quoted in the text where appropriate.

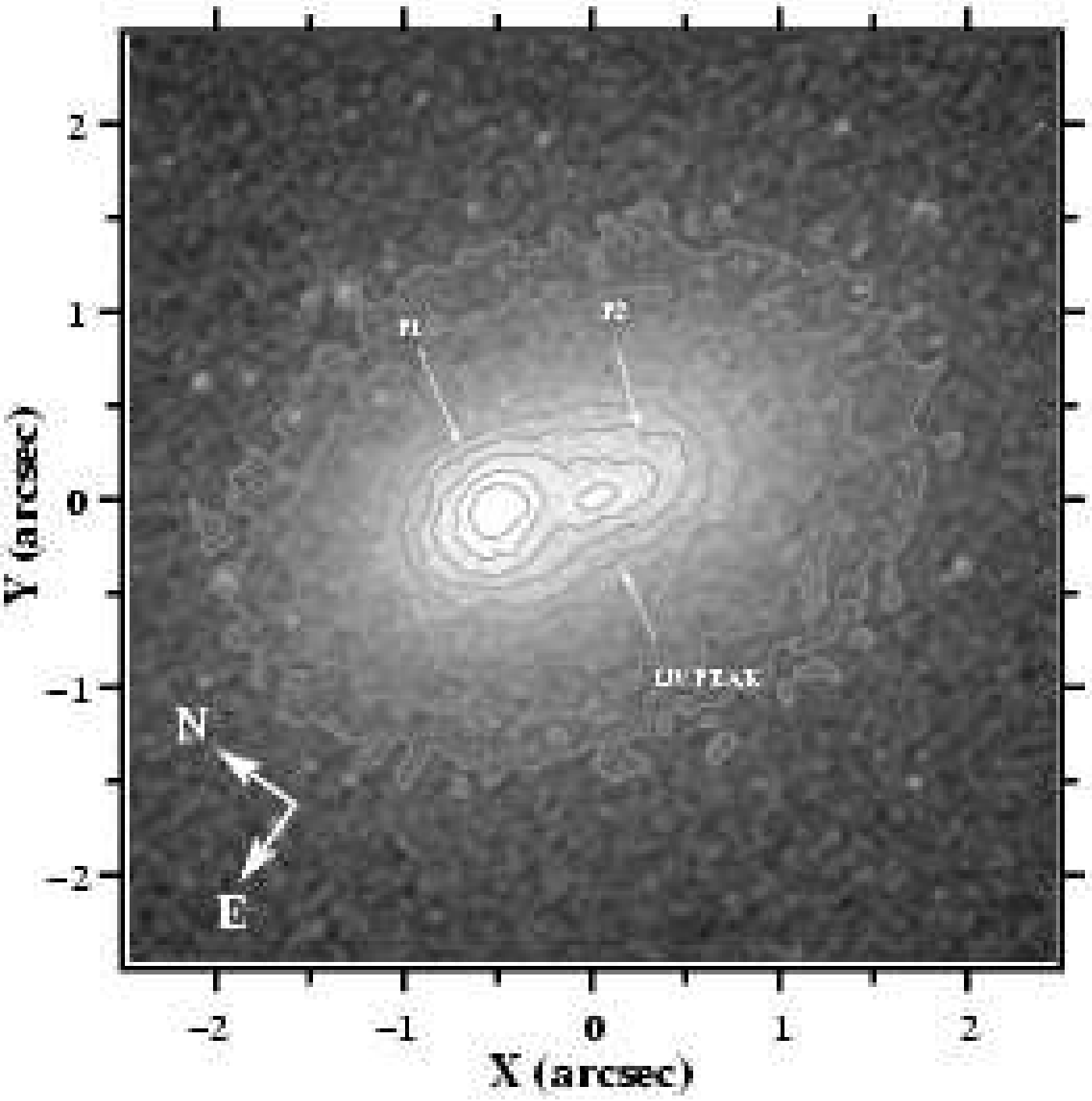

FIG. 1.— A deconvolved (L98) grey scale image of the M31 double nucleus in the $V(F555W)$ band. The intensity stretch is logarithmic, and the contour interval is 0.2 mag.

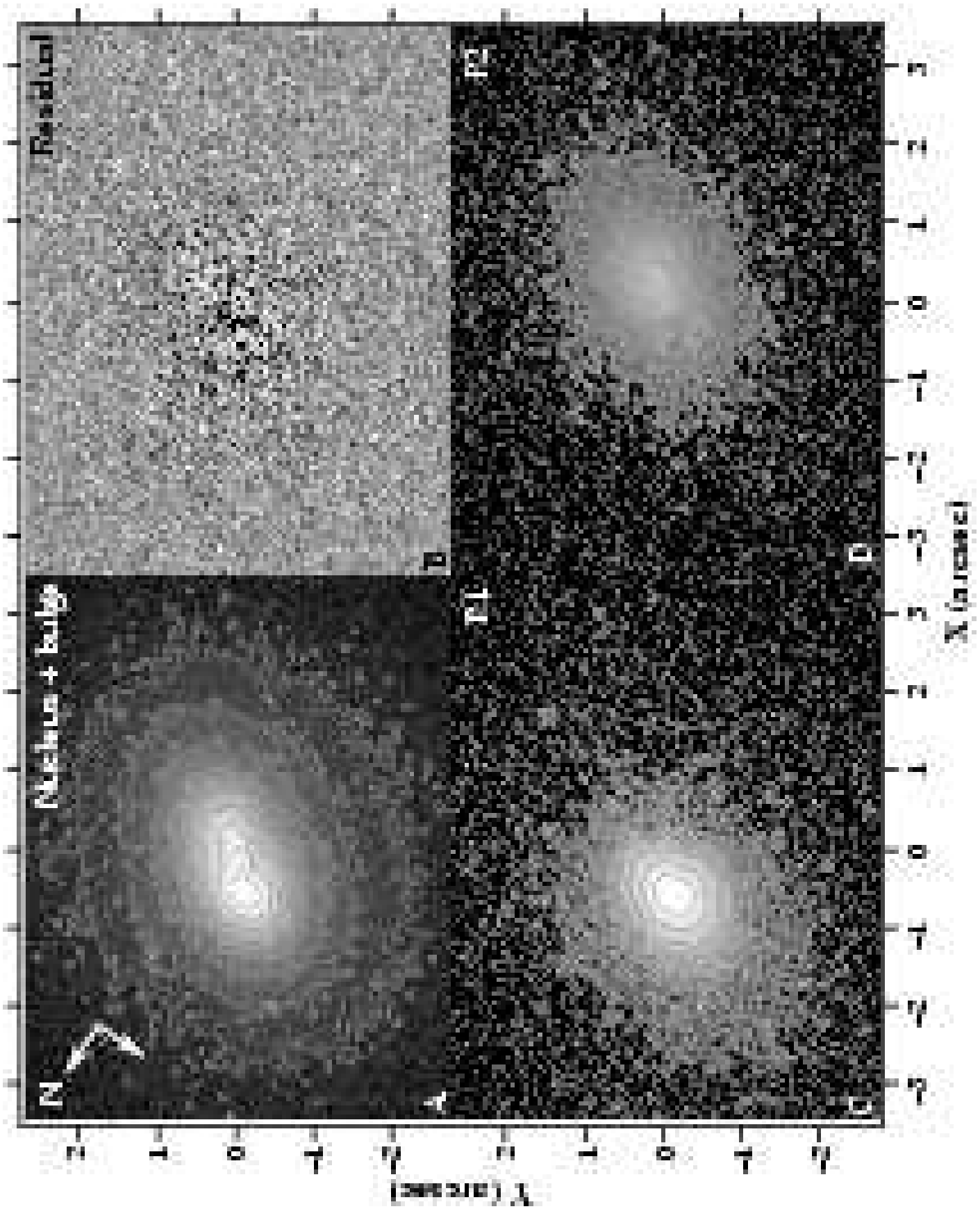

FIG. 2.— Decomposition of M 31.(a) bulge + nucleus. (b) residuals from 2-D GALFIT are shown in positive grey scale. (c) P1 component. (d) P2 component. The contour intervals are arbitrary.

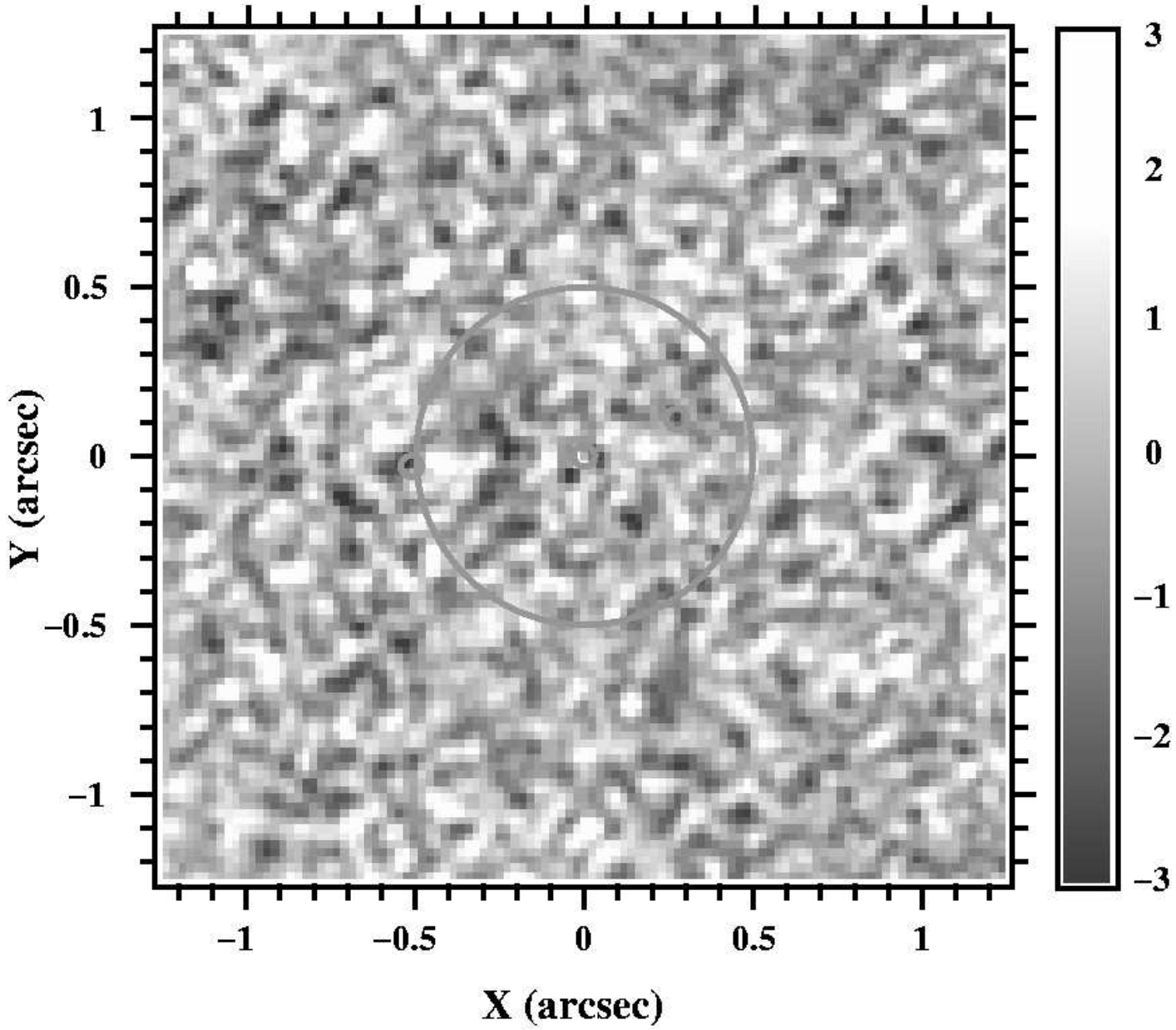

FIG. 3.— Image of the fit residuals divided by the local RMS, with intensity scale shown to the right. The calculation of the RMS image is discussed in § S3.2. The large circle has a radius of 0.″5 centered on the UV peak (small central circle). The other two circles at (−0.″51, −0.″02) and (0.″28, 0.″1) represent the position of P1 (left) and P2 (right), respectively. The image orientation is the same as Figs. 1 and 2.

TABLE 2
NUCLEAR LUMINOSITY/MASS DENSITY PARAMETERS

Bulge Type	$\langle\gamma\rangle$ ($r < 0''.1$)	$\langle\gamma\rangle$ ($r < 10$pc)	$\log\langle j\rangle$ ($r < 0''.1$)	$\log\langle j\rangle$ ($r < 10$pc)	$\log\langle\rho\rangle$ ($r < 0''.1$)	$\log\langle\rho\rangle$ ($r < 10$pc)	$\langle\psi\rangle$ ($r < 0''.1$)	$\langle\psi\rangle$ ($r < 10$pc)
(1)	(2)	(3)	(4)	(5)	(6)	(7)	(8)	(9)
Nuker	0.14	0.15	3.97	2.65	4.73	3.41	1.16	1.12
Sérsic	0.01	0.03	3.33	2.59	4.09	3.35	0.51	0.51

Note. — Col. (1): The bulge is defined as the sum of two components described in the text: the spherical + Nuker, or spherical + Sérsic. Col. (2 and 3): The average logarithmic power law slope of the bulge surface brightness ($\langle d\log I/d\log r\rangle$) within $r < 0''.1$ and 10pc. Col. (4 and 5): The logarithmic average luminosity density j integrated within $r < 0''.1$ and 10pc, in units of $[L_\odot/\mathrm{pc}^3]$. Col. (6 and 7): The logarithmic mass density ρ inferred from Col. 4 and 5, in units of $[M_\odot/\mathrm{pc}^3]$, based on $M/L = 5.7$. Col. (8 and 9): The average mass density power law slope ψ ($\langle d\log\rho/d\log r\rangle$), analogous to $\langle\gamma\rangle$.

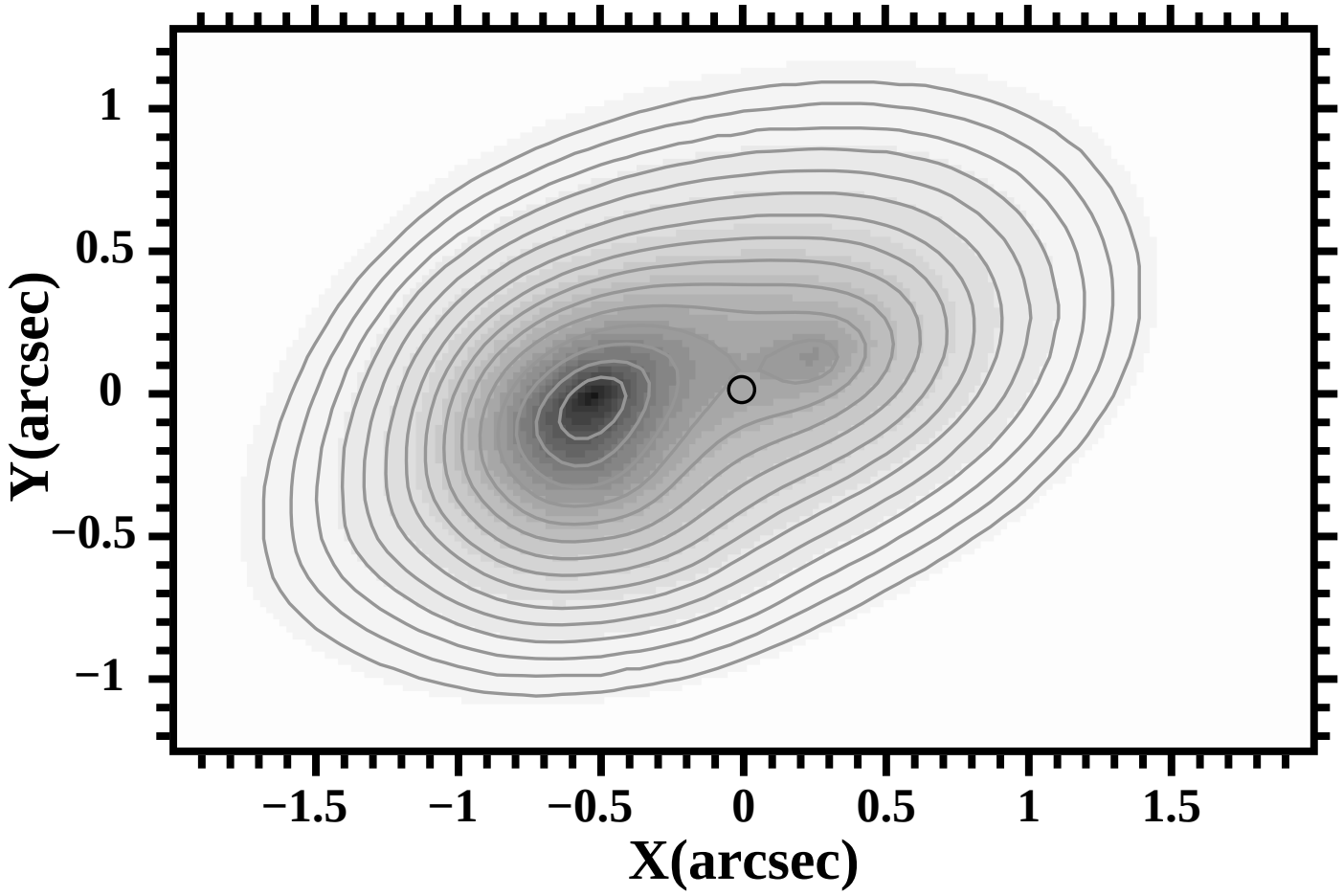

FIG. 4.— Model of the eccentric disk, P1 and P2. The position of the UV peak is marked by a circle at the center. The contour interval is 0.1 magnitude.

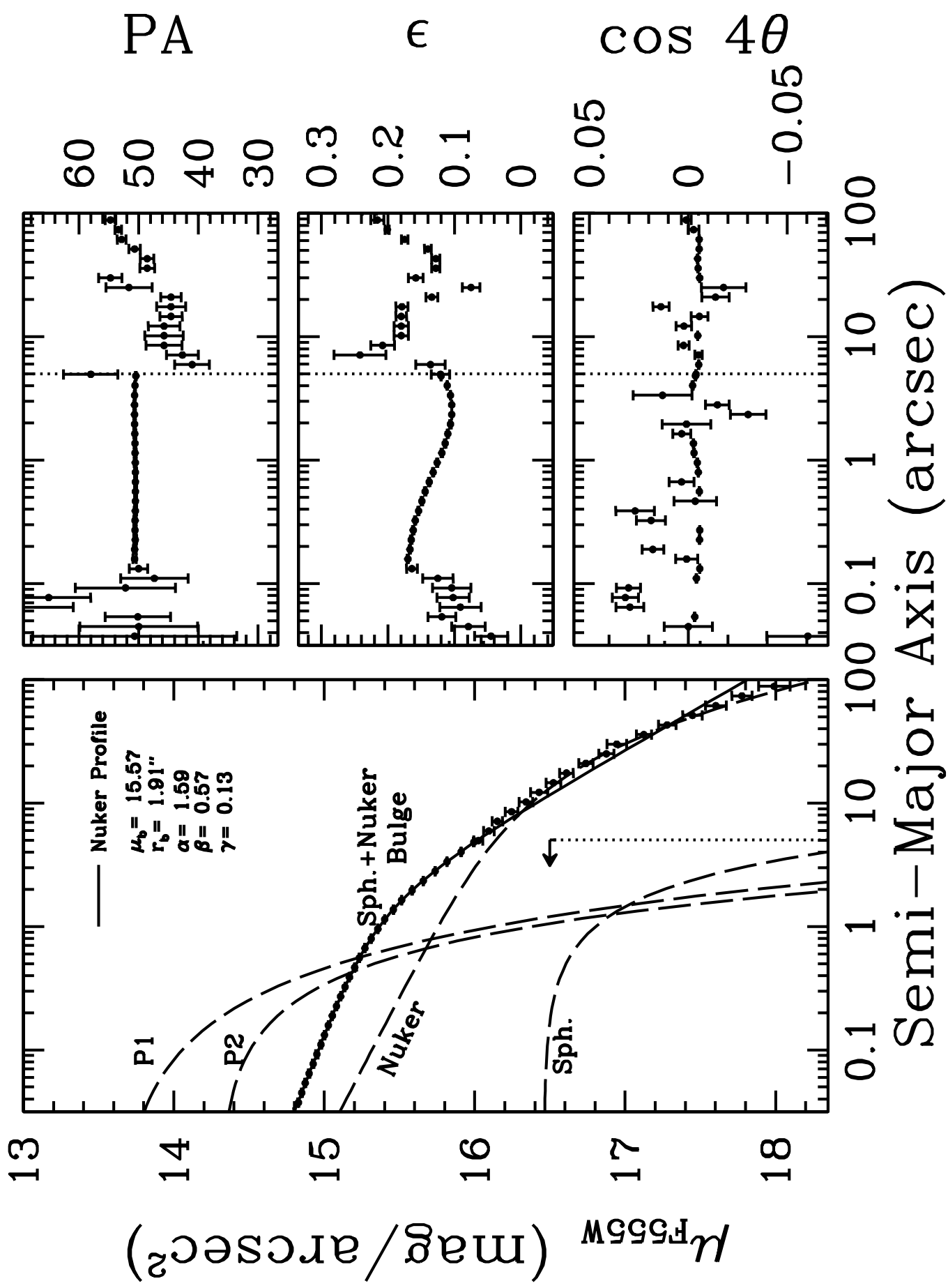

FIG. 5.— Isophote fits to the WFPC2 mosaic image. The surface brightness profile panel shows the "intrinsic" bulge profile as data points. Inner to 5″, marked by vertical dotted lines, the double nucleus begins to dominate, so we replace that region by a sum of the fitted Nuker + spherical bulge components (see text). The profile of the individual components used in the fit are shown in dashed lines. The solid line

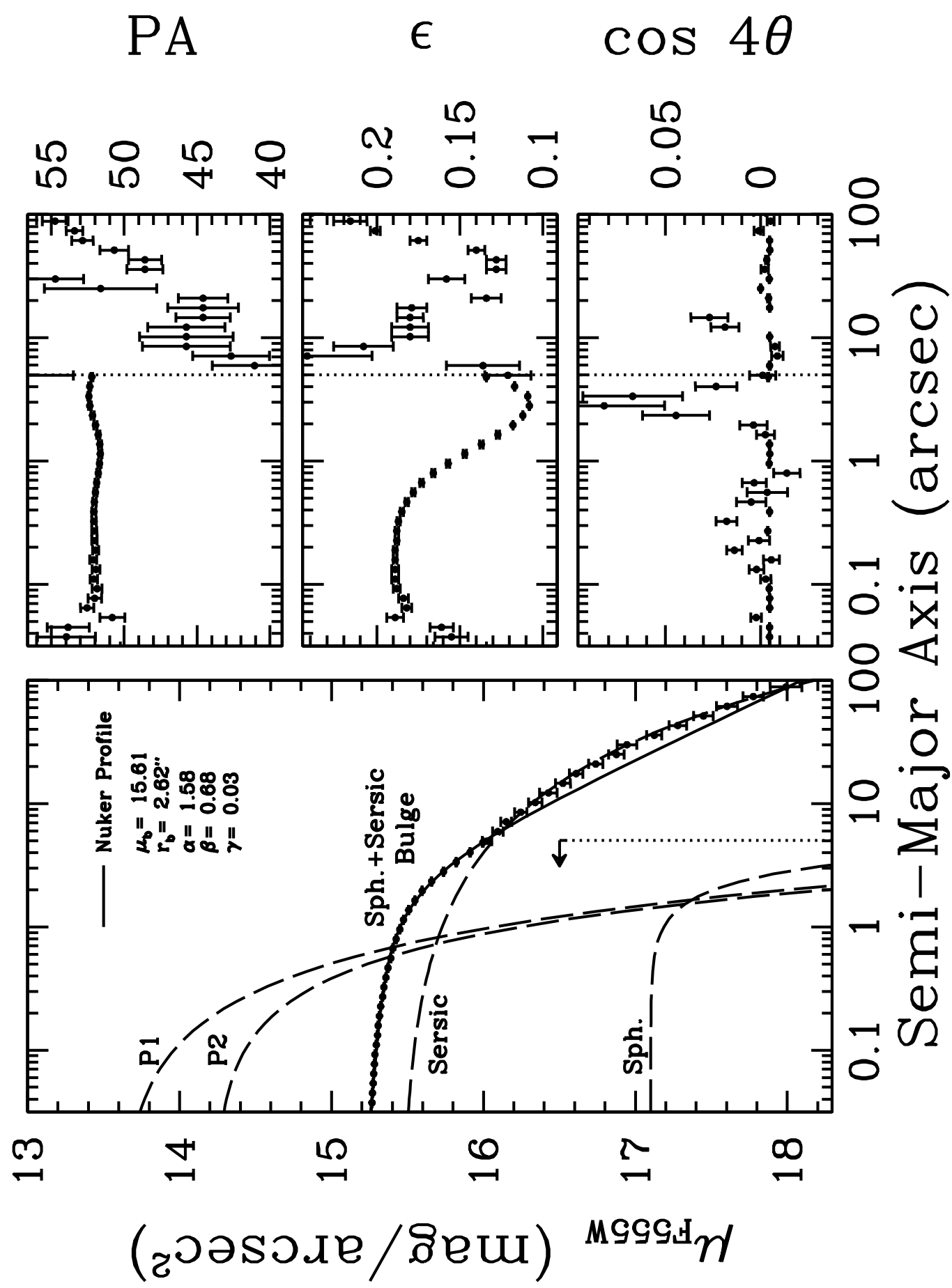

FIG. 6.— Isophote fits to the WFPC2 mosaic image. The surface brightness profile panel shows the "intrinsic" bulge profile as data points. Inner to 5″, marked by vertical dotted lines, the double nucleus begins to dominate, so we replace that region by a sum of the fitted Sérsic + spherical bulge components (see text). The profile of the individual components used in the fit are shown in dashed lines. The solid line

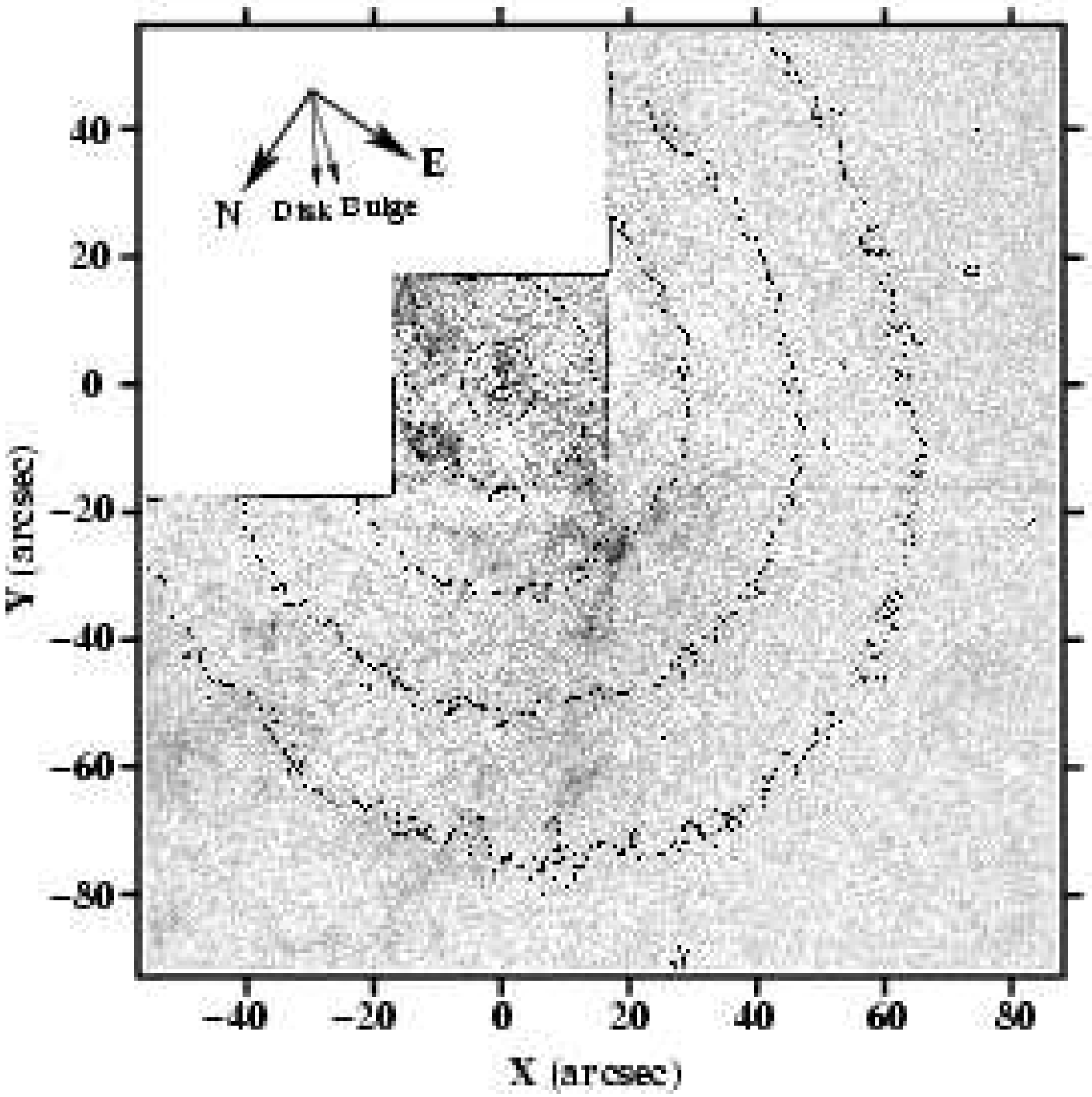

FIG. 7.— A residual image with the bulge and nucleus subtracted, showing a dust lane that runs clear through the center. The isophotes superposed are from the same image before subtraction, and have logarithmic spacing. The compass shows the orientation of the image with respect to the sky, as well as the major axis orientation of the M31 galactic disk and large scale bulge.

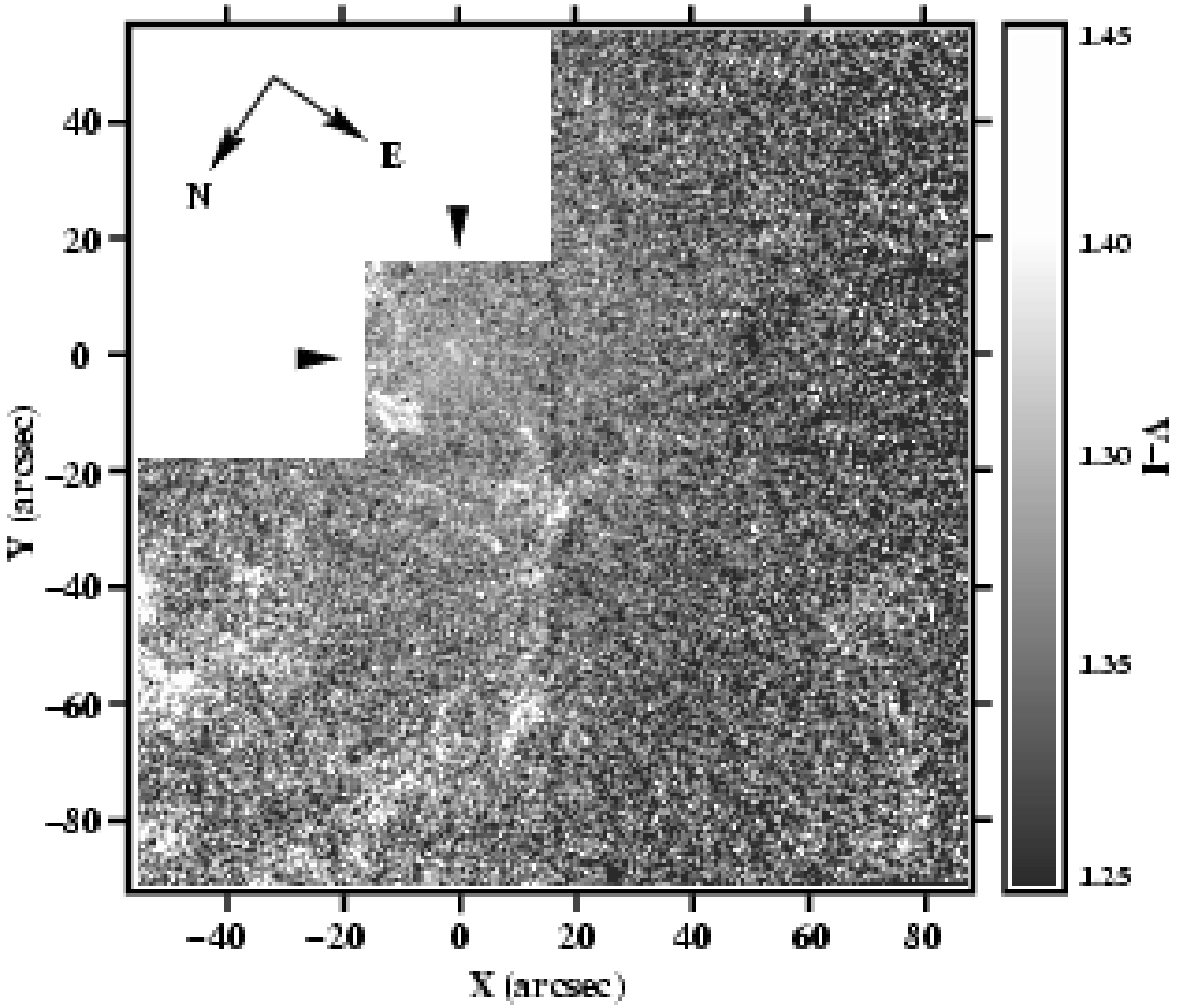

FIG. 8.— A $(V - I)$ color map showing color gradient of the bulge. The arrowheads mark the location of the double nucleus. The image has been smoothed over by a Gaussian kernel of $\sigma = 2$ pixels.